Design criteria for microstructured-optical-fiber-based surface-plasmon-resonance sensors

Alireza Hassani and Maksim Skorobogatiy

Department of Engineering Physics, École Polytechnique de Montréal, Case Postale 6079, succ. Centre-Ville Montreal, Québec H3C3A7, Canada

Received October 4, 2006; revised February 8, 2007; accepted February 10, 2007; posted March 2, 2007 (Doc. ID 75698); published May 17, 2007

Design strategies for microstructured-optical-fiber (MOF-) based surface-plasmon-resonance (SPR) sensors are presented. In such sensors, plasmons on the inner surface of the large metallized channels containing analyte can be excited by a fundamental mode of a single-mode microstructured fiber. Phase matching between a plasmon and a core mode can be enforced by introducing air-filled microstructures into the fiber core. Particularly, in its simplest implementation, the effective refractive index of a fundamental mode can be lowered to match that of a plasmon by introducing a small central hole into the fiber core. Resolution of the MOF-based sensors is demonstrated to be as low as 3×10^{-5} RIU, where RIU means refractive index unit. The ability to integrate large-size microfluidic channels for efficient analyte flow together with a single-mode waveguide of designable modal refractive index is attractive for the development of integrated highly sensitive MOF-SPR sensors operating at any designable wavelength.

OCIS codes: 130.6010, 240.6680, 060.2370.

1. INTRODUCTION

Propagating at the metal–dielectric interface, surface plasmons[1] are extremely sensitive to changes in the refractive index of the dielectric. This feature constitutes the core of many surface-plasmon-resonance (SPR) sensors. Typically, these sensors are implemented in the Kretschmann–Raether prism geometry to direct *p*-polarized light through a glass prism and reflect it from a thin metal (Au, Ag) film deposited on the prism facet.[2] The presence of a prism allows resonant phase matching of an incident electromagnetic wave with a high-loss plasmonic wave at the metal–analyte interface at a specific combination of the angle of incidence and wavelength. By detecting changes in the amplitude or phase of the reflected light due to its coupling with a plasmon wave, one can detect minute changes in the refractive index of an analyte bordering the metal layer. Using optical fibers instead of a prism in plasmonic sensors offers miniaturization, a high degree of integration, and remote sensing capabilities. Over the past decade, driven by the need of miniaturization of SPR sensors, various compact configurations enabling coupling between optical waveguide modes and surface-plasmonic waves have been investigated. Among others, metallized single-mode, polarization maintaining, and multimode waveguides, metallized tapered fibers, and metallized fiber Bragg gratings have been studied.[3–21] Two principal difficulties hindering development of the integrated waveguide-based sensors have been identified.

The first challenge is phase matching of a waveguide core mode and a plasmonic wave. Mathematically, phase matching constitutes equating the effective refractive indexes of the two modes at a given wavelength of operation. In the case of a single-mode waveguide, the effective refractive index of its core mode is close to that of a core material. For most practical core materials, such indices are higher than 1.45. The effective refractive index of a plasmon is typically close to that of a bordering analyte, which in the case of air is ~1.0, while in the case of water is ~1.33. Only at higher frequencies[7,10] ($\lambda<700$ nm for a plasmon on a gold metal film, for example) the plasmon refractive index becomes high enough to match that of a waveguide core mode. From a sensor design point of view, it is quite unsatisfactory to be limited by the values of the material refractive indices without the ability of compensating material limitations with a judicious choice of a sensor geometry. In principle, the phase-matching problem can be alleviated by coupling to a plasmon via the high-order modes of a multimode waveguide.[18–21] Such modes can have significantly lower effective refractive indices than a waveguide core index. In such a setup, light has to be launched into a waveguide to excite high-order modes, some of which will be phase matched with a plasmon mode. As only a fraction of higher-order modes are phase matched to a plasmon, then only a fraction of total launched power will be coupled to a plasmon, thus reducing sensor sensitivity. Moreover, as power distribution in high-order modes is very sensitive to the launching conditions, this adds additional noise due to variations in a coupling setup.

The second problem that limits development of the waveguide-based sensors is that of packaging of the microfluidics setup, waveguide, and metallic layers into a single sensor. For example, in traditional single-mode fiber-based sensors, to metallize fiber surfaces, one has to first strip the fiber jacket and then polish fiber cladding almost to the core to enable evanescent coupling with a plasmon. This laborious procedure compromises fiber integrity, making the resulting sensor prone to mechanical failures. Integration of a metallized fiber piece into a mi-

crofluidics setup presents yet another additional step in sensor fabrication, thus increasing the overall fabrication cost.

The goal of this paper is to build upon a great body of ideas developed by the waveguide-based SPR sensing community and to illustrate that the phase-matching and packaging issues can be facilitated using photonic crystal fibers (PCFs) or microstructured optical fibers (MOFs) operating in the effectively single-mode regime. Recently, we have demonstrated that the effective refractive index of a Gaussian-like core mode propagating in the bandgap of a photonic crystal waveguide[22,23] can be designed to take any value from 0 to that of a refractive index of a core material. This enables phase matching and plasmon excitation by the waveguide core mode at any desirable wavelength. It was also recently demonstrated[24,25] that the plasmon mode can be excited by the core-guided mode of a single-mode holey fiber featuring a single ring of metallized holes. Microfluidics in microstructured fibers is enabled by passing analyte though the fiber porous cladding, thus, partially solving the packaging problem. Deposition of metal layers inside of the MOFs can be performed either with the high-pressure chemical vapor deposition technique[26] or electroless plating techniques used in fabrication of metallized hollow waveguides and microstructures.[27,28]

2. GEOMETRY OF A MICROSTRUCTURED-OPTICAL-FIBER-BASED SURFACE-PLASMON-RESONANCE SENSOR

In this paper, we develop general principles of the MOF design for applications in plasmonic sensing, where the two key requirements are phase matching with a plasmon wave and optimized microfluidics. Figures 1(a) and 1(b) show the two schematics of proposed hexagonal solid-core MOF-based SPR sensors. In the first MOF, the fiber core is surrounded by the two layers of holes. Metallized holes in the second layer are considerably larger than those in the first layer, thus simplifying the flow of analyte through them. This fiber has been considered in detail in Ref. 25. In the second MOF, two large semicircular channels covered with metal are used to further enhance microfluidic flow. Another reason for the introduction of the two structures is to study the effect of metallic surface geometry on the efficiency of plasmonic excitation.

To lower the refractive index of a core-guided mode (to facilitate phase matching with a plasmon), we introduce a small hole of diameter d_c into the core center. In place of a single hole in the core, an array of smaller holes can be used similar to those in Ref. 29. Holes in the core and in the first layer are filled with air $n_{\text{air}}=1.0$, while metal-covered holes in the second layer are filled with analyte (aqueous solution) $n_a \simeq 1.33$. As a first example, we will consider a MOF with the diameters of the core, first-, and second-layer holes chosen as $d_c=0.5\Lambda$, $d_1=0.6\Lambda$, and $d_2=0.8\Lambda$, respectively. The pitch of the underlying hexagonal lattice is $\Lambda=2$ μm. By changing the size of a central hole, one can tune the effective refractive index of the fundamental mode. The first layer of holes works as a low refractive index cladding enabling mode guidance in the fiber core. Coupling strength between the core mode and plasmon is strongly influenced by the size of the holes in the first layer (larger hole sizes result in a weaker coupling). Holes in the second layer of Fiber I and semicircular channels of Fiber II are metallized with an ~40 nm layer of gold and feature large sizes to facilitate the flow of analyte. Finally, we assume that MOF is made of a silica glass with the refractive index given by the Sellmeier equation. The dielectric constant of gold ϵ_{Au} is approximated in the visible and near-IR region by the Drude model[30] $\epsilon_{\text{Au}}(\omega)=\epsilon^{\infty}-\omega_p^2/[\omega(\omega+i\omega_\tau)]$, where $\epsilon^{\infty}=9.75$, $\omega_p=1.36\times10^{16}$ rad/s, and $\omega_\tau=1.45\times10^{14}$ rad/s.

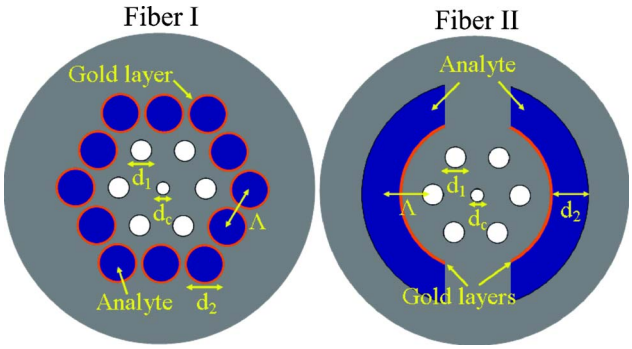

Fig. 1. (Color online) Schematics of the two MOF-based SPR sensors. In Fiber I, large holes in the second layer are filled with analyte and metallized for plasmon excitation. Air-filled holes in the first layer enable guiding in the higher refractive index fiber core, while at the same time, control coupling strength between the core mode and plasmon wave. A small air-filled hole in the fiber core is used to lower the refractive index of a core-guided mode to facilitate phase matching with a plasmon. In Fiber II, a large semicircular metallized channel is integrated into the fiber structure to enhance microfluidic flow.

3. EXCITATION OF PLASMONIC WAVES BY THE CORE-GUIDED MODE OF A MICROSTRUCTURED OPTICAL FIBER

A finite-element method with perfectly matched layer boundaries was used to find complex propagation constants of the core-guided and plasmonic modes. A typical fiber-based plasmonic sensor operates in the vicinity of a phase-matching point between the core-guided mode and a plasmon wave localized at the metallized surface. As an example, in Fig. 2 for Fiber II, we present dispersion relations of the core-guided mode (solid curve) and a plasmon wave (dashed curve). The phase-matching point is located at 640 nm, where the difference between the modal refractive indexes is the smallest. Energy flux distributions in the vicinity of a phase-matching point [insets (a) and (b) in Fig. 2] allow clear differentiation of the nature of the two modes. In the vicinity of a phase-matching point, the two modes become strongly mixed [inset (c) in Fig. 2], with losses of a core-guided mode increasing dramatically due to the energy transfer into the lossy plasmon mode. Core-mode losses, which are proportional to $\text{Im}(N_{\text{eff}})$, are presented in Fig. 2 in a thin solid curve. For reference, losses in decibels per meter are defined as $\alpha(\text{dB/m})=40\pi\,\text{Im}(N_{\text{eff}})/(\ln(10)\lambda\ \text{m})$, where λ is in meters. Detection of increase in the loss of a core-guided mode at the point of its phase matching with a plasmon constitutes the heart of many sensor designs.

We now investigate a plasmon-wave transduction mechanism in greater detail. In Fig. 3, we present losses of the core-guided modes in the wavelength range of 0.5–1.3 μm for the two MOF designs of Fig. 1. The thin solid curve corresponds to Fiber I, filled with analyte of $n_a=1.33$, and features three plasmonic excitation peaks located at 560, 950, and 1290 nm defined by increase in the core-mode propagation losses. The thick solid curve corresponds to Fiber II, filled with the same analyte of $n_a=1.33$, and features two plasmonic excitation peaks located at 640 and 1120 nm. To demonstrate potential of these fibers for sensing, we present in thin and thick dashed curves, losses of the core-guided modes of Fibers I and II for the case when the analyte refractive index is slightly varied ($n_a=1.34$ for Fiber I, and $n_a=1.335$ for Fiber II). As a result, positions of the plasmonic resonances shift by ~10 nm, with the first peak (at shorter wavelengths) being the most sensitive to the changes in the analyte refractive index. This transduction mechanism is commonly used for detecting the analyte bulk refractive index changes, as well as monitoring formation of the nanometer-thin biolayers on top of a metallized sensor surface.

It is important to note that the shape of a metallized surface can have a significant effect on the plasmonic excitation spectrum. Thus, a planar metallized surface supports only one plasmonic peak, while a cylindrical metal layer can support several plasmonic peaks.[12,14,15,31] In Fig. 3, we present energy flux distributions at the first and second plasmonic peaks of the two MOFs considered in this paper. From the pictures, one can see that the shape of a metallized surface strongly affects the field distributions of plasmonic waves. Moreover, one can also notice that for the first plasmonic peaks, there is considerably more field penetration into the analyte-filled channels than in the case of the second plasmonic peaks. This explains why center wavelengths of the first peaks are considerably more sensitive than the center wavelengths of the second peaks to the changes in the analyte refractive index. In principle, by monitoring changes in

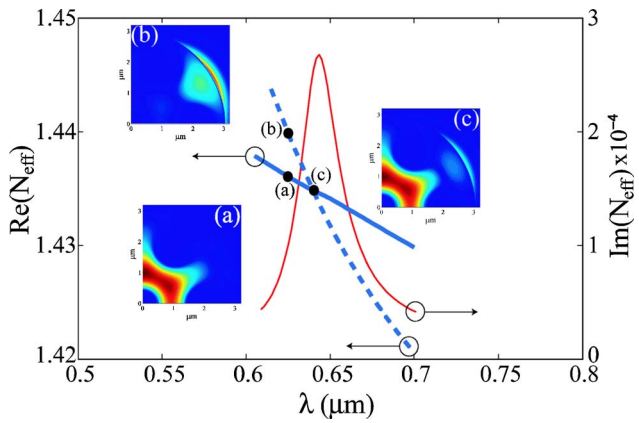

Fig. 2. (Color online) Dispersion relations of a core-guided mode (thick solid curve) and a surface plasmon (thick dashed curve) in the vicinity of the phase-matching point. Insets (a) and (b) show energy fluxes of the core-guided and plasmon modes close to the phase-matching point. Transmission loss of a core-guided mode (thin solid curve) exhibits a strong increase at the phase-matching point due to efficient mixing with a plasmon wave as confirmed by its energy flux distribution [inset (c)].

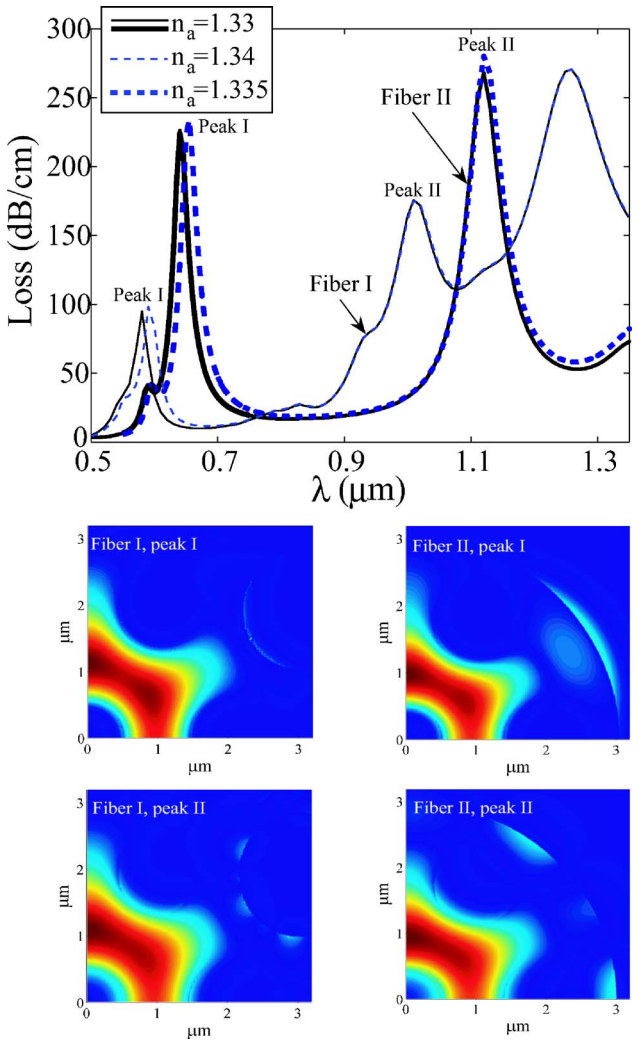

Fig. 3. (Color online) Calculated loss spectra of the core-guided modes for two fiber designs. Loss spectra (solid curves) feature several attenuation peaks corresponding to the excitation of plasmonic modes on the surface of metallized channels filled with aqueous analyte $n_a=1.33$. By changing analyte refractive index (dotted curves) resonant attenuation peaks corresponding to the points of phase matching between the core-guided and plasmon modes shift. In the insets, energy flux of a core-guided mode is presented at various absorption peaks.

the excitation of several plasmonic resonances, one can improve sensor sensitivity. With this method, refractive index resolution of $\sim 10^{-6}$ has been demonstrated in optical fibers covered with circular metallic layers.[15]

The plasmon wave, being a surface excitation, is also very sensitive to the thickness of a metallic layer. In Fig. 4, we show changes in the spectra of the first plasmonic peaks for Fibers I and II when the thickness of a gold layer on the inside of microfluidic channels is varied. Generally, modal propagation loss at resonance decreases when thickness of a gold layer increases, and simultaneously, center wavelengths of the peaks shift toward longer wavelengths. For Fiber II, for example, the position of a plasmonic peak shifts from 640 to 655 nm when the gold layer thickness increases from 40 to 65 nm. Given that the width of a peak at half maximum is ~40 nm, changes in the peak position due to nanometer variations in the metal layer thickness can be easily de-

tected. This transduction mechanism can be used to study metal nanoparticle binding events on the metallic surface of a sensor.[32] This mode of sensor operation can be of interest, for example, to the monitoring of concentration of metal nanoparticles attached to the photosensitive drugs in photodynamic cancer therapy.[33]

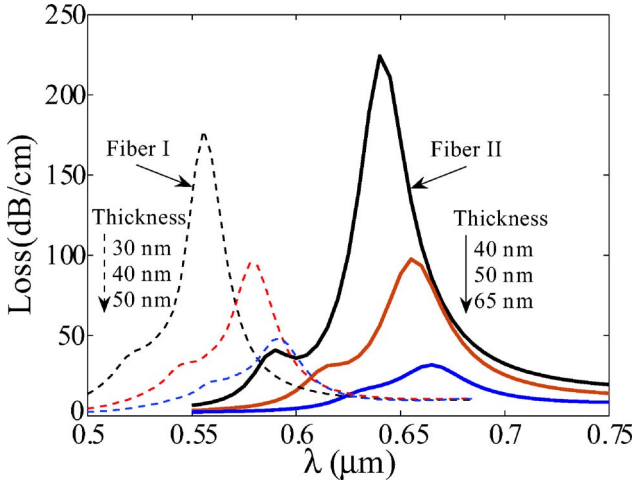

Fig. 4. (Color online) Loss spectra in the vicinity of the first plasmonic peak for fibers with a gold layer of varying thickness. Dashed curves—Fiber I, solid curves—Fiber II.

4. TUNING OF PLASMONIC EXCITATIONS

A plasmon-wave excitation spectrum can be readily tuned by varying MOF structural parameters. In what follows, we will study the effect of size variation of the central hole, as well as holes in the first layer, with a view of tuning and optimizing plasmon excitation by the core-guided mode of a MOF.

In Figs. 5(a) and 5(b) we present losses and effective refractive indexes of a core-guided mode of Fiber II in the vicinity of a plasmonic Peak I for various diameters of the central hole $d_c=0.55\Lambda$, 0.45Λ, and 0.35Λ. The diameter of the holes in the first layer is fixed and equal to $d_1=0.6\Lambda$. In Fig. 5(a), one can observe an overall increase in the modal losses of a core-guided mode for the larger diameters of the central hole. This fact is easy to rationalize by noting that the larger size of a central hole promotes expulsion of the modal field from the fiber core. This, in turn, leads to the greater modal presence near the metallic interface, hence higher propagation losses. Another consequence of the modal expansion from the fiber core and into the air-filled microstructure is reduction of the modal refractive index, leading to the shift of a plasmonic peak toward longer wavelengths.

In Fig. 5(c), we present losses of a core-guided mode of Fiber II in the vicinity of plasmonic Peak I for various diameters of the holes in the first layer $d_1=0.6\Lambda$, 0.7Λ. The

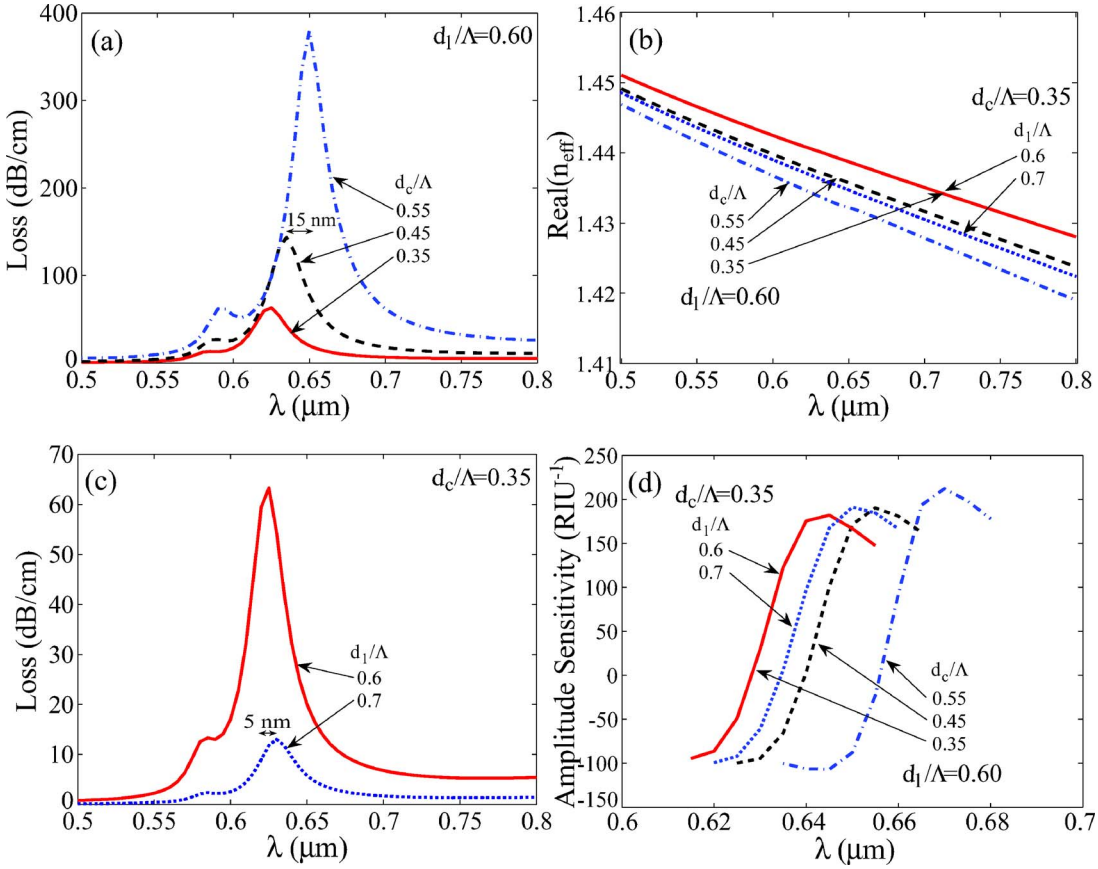

Fig. 5. (Color online) Effect of the fiber structural parameters on the efficiency of plasmon excitation (case of Fiber II, incorporating a 40 nm thick gold layer). (a) Loss of a core-guided mode for various values of the fiber central hole diameter $d_c=0.55\Lambda, 0.45\Lambda, 0.35\Lambda$, assuming a fixed diameter of the first layer holes $d_1=0.6\Lambda$. (b) Dispersion relation of a fiber core mode for various values of the structural parameters. (c) Loss of a core-guided mode for two values of the first layer hole diameter $d_1=0.6\Lambda, 0.7\Lambda$, assuming a fixed central hole diameter $d_c=0.35\Lambda$. (d) Sensitivity comparison between fibers of different structural parameters.

diameter of the central hole is fixed and equal to $d_c = 0.35\Lambda$. In Fig. 5(c), one can observe an overall decrease in the modal losses of a core-guided mode for the larger size holes in the first layer. This is easy to understand by noting that larger sized holes in the first layer lead to the lower refractive index of the microstructured cladding. This, in turn, increases the core-cladding refractive index contrast, hence increasing modal confinement in the core region, and resulting in lower modal losses due to coupling to a metal surface in the second layer.

5. SENSITIVITIES OF MICROSTRUCTURED-OPTICAL-FIBER-BASED-SURFACE-PLASMON-RESONANCE SENSORS

The simplest mode of operation of a fiber-based SPR sensor is the detection of changes in the bulk refractive index of an analyte. As the real part of a plasmon refractive index depends strongly on the value of an analyte refractive index, the wavelength of phase matching between the core-guided and plasmon modes will also be sensitive to the changes in the analyte refractive index. There are two main approaches to detection. The first one is an amplitude-(or phase-) based method, where all of the measurements are done at a single wavelength. The advantage of this method is its simplicity and low cost as no spectral manipulation is required. The disadvantage is a smaller operational range and lower sensitivity when compared with the wavelength interrogation methods, in which transmission spectra are taken and compared before and after the change in the analyte has occurred.

We start by describing a single wavelength, amplitude-based detection method. We define $\alpha(\lambda, n_a)$ to be the transmission loss of a core mode as a function of the wavelength and refractive index of an analyte. Considering P_0 to be the power launched into the fiber core mode, the power detected after propagation along the sensor of length L will be $P(L,\lambda,n_a)=P_0\exp(-\alpha(\lambda,n_a)L)$. For the operational wavelength λ, amplitude sensitivity to the dn_a change in the analyte refractive index can then be defined as $S_A(\lambda)$ $(\mathrm{RIU}^{-1})=|P(L,\lambda,n_a+dn_a) - P(L,\lambda,n_a)|/P(L,\lambda,n_a)/dn_a$, which is frequently expressed in the units of $\mathrm{dB\,RIU}^{-1}$ defined as $S_A(\lambda) \times(\mathrm{dB\,RIU}^{-1})=10/\ln(10)S_A(\lambda)(\mathrm{RIU}^{-1})$. The sensor length L is limited by the modal transmission loss. A reasonable choice of sensor length is $L=1/\alpha(\lambda,n_a)$, which falls into a subcentimeter range for the MOFs described in this paper. The corresponding sensor volume is then subnanoliter. This choice of a sensor length results in a simple definition of sensitivity for the small changes in the analyte refractive index:

$$S_A(\lambda)(\mathrm{RIU}^{-1}) = |\partial\alpha(\lambda,n_a|/\partial n_a)/\alpha(\lambda,n_a).$$

In Fig. 6, we present amplitude sensitivities of the two proposed MOF-SPR sensors for the various values of the metal layer thickness 40, 50, and 65 nm. Dashed curves correspond to the Fiber I-based sensor, while solid curves correspond to the Fiber II-based sensor. Maximum sensitivity of the Fiber I-based sensor for detecting changes in the aqueous analyte in the vicinity of 0.6 μm is 520 $\mathrm{dB\cdot RIU}^{-1}$, while maximum sensitivity of a Fiber II-based sensor in the vicinity of 0.65 μm is 820 $\mathrm{dB\,RIU}^{-1}$. It

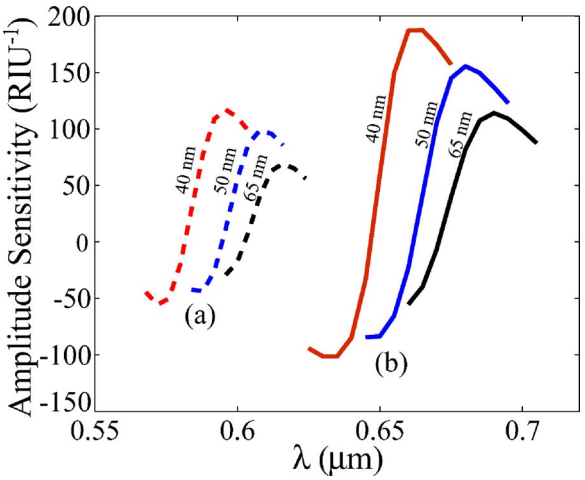

Fig. 6. (Color online) Sensitivity of the two MOF-based sensors in the vicinity of the first plasmonic peak for various values of the gold layer thickness. Dashed curves—Fiber I, solid curves—Fiber II.

is typically a safe assumption that a 1% change in the transmitted intensity can be detected reliably, which leads to the sensor resolutions of 8×10^{-5} RIU and 5×10^{-5} RIU for the fiber Designs I and II, respectively. Predicted sensitivities of our fiber designs are comparable with the ones of the best existing fiber sensors.[34]

Note from Fig. 6 that amplitude sensitivity depends strongly on the thickness of a gold layer. Overall, sensitivity decreases when the metallic layer becomes thicker. This fact is simple to understand. When the metallic layer thickness becomes significantly larger than that of a metal skin depth (~20–30 nm), the fiber core mode becomes effectively screened from a plasmon, resulting in a low coupling efficiency, and, as a consequence, low sensitivity. Additionally, as the fiber material refractive index is larger than that of an analyte, for thicker metal layers, the plasmon refractive index decreases. In accordance with Fig. 5(b), this leads to a shift of the sensitivity peak (phase-matching wavelength) toward longer wavelengths. Rather surprisingly, the maximum value of sensitivity is only weakly dependent on the choice of the diameters of the central and first layer holes. In Fig. 5(c), we present amplitude sensitivity of the Fiber II-based design for various choices of the d_c and d_1 parameters. While impacting strongly on the wavelength of peak sensitivity and the value of the modal loss, various choices of hole diameters have a weak effect on the maximum value of sensitivity. As sensor length is inversely proportional to the modal loss, tuning of the fiber structural parameters allows design of fiber sensors of widely different lengths (from millimeter to meter), while having comparable sensitivities. This might be important for the practical considerations of integrating such a fiber-sensing element into a complete sensor system.

In the wavelength interrogation mode, changes in the analyte refractive index are detected by measuring displacement of a plasmonic peak. In this case, sensitivity is defined as S_λ $(\mathrm{nm\,RIU}^{-1})=|d\lambda_{\mathrm{peak}}/dn_a|$. For the two MOF-based designs with a 40 nm gold layer, we find that their corresponding sensitivities are 800 $\mathrm{nm\,RIU}^{-1}$ and 3000 $\mathrm{nm\,RIU}^{-1}$, respectively. It is typically a safe assump-

tion that a 0.1 nm change in the position of a resonance peak can be detected reliably, which leads to the sensor resolutions of 1.2×10^{-4} RIU and 3×10^{-5} RIU for fiber Designs I and II, respectively. Again, as in the case of amplitude-based sensors, we find that for measuring changes in the aqueous analyte using the wavelength interrogation mode, sensitivities of our sensors are comparable to the ones of the best existing waveguide sensors.[34]

6. CONCLUSION

We have introduced a concept of MOF-based SPR sensors. Two main sensor design challenges were identified, which are the phase matching of the core-guided and plasmonic modes, and microfluidics optimization to enable efficient analyte flow. Phase matching was facilitated by the introduction of the hollow microstructure into the fiber core. Improved microfluidics was addressed by the integration of large analyte-filled channels adjacent to the fiber core. Detection limit of the amplitude-based sensor for measuring changes in the aqueous analyte at 0.65 μm was found to be 5×10^{-5} RIU, assuming a 1% amplitude change detection limit. The detection limit of the same sensor in the wavelength interrogation mode was found to be 3×10^{-5} RIU, assuming a 0.1 nm detection limit in the shift of a plasmonic peak. Thus the found sensitivities are comparable to the ones of the best existing fiber and waveguide-based sensors optimized for aqueous analytes. Additionally, MOFs offer sensor design at almost any desirable wavelength in the visible and near IR because of their ability to support core-guided modes of small effective refractive indices. By adjusting many of the MOF geometrical parameters it is considerably simpler to enforce phase matching with a plasmon compared with standard total internal reflection waveguides and fibers. Moreover, integration of the microfluidic channels during MOF drawing increases sensor reliability as the laborious extra step of microfluidics packaging is avoided.

ACKNOWLEDGMENTS

We thank A. Kabashin for his insights into the possible modes of operation of MOF-based plasmonic sensors; M. Koshiba, K. Saitoh, and S. K. Varshney for in-depth discussion of the finite-element method in application to the analysis of plasmonic sensors; and Canada Research Chair, the Natural Sciences and Engineering Research Council, Le Fonds Québécois de recherche sur la nature et le technologies, and the Canadian Institute for Photonic Innovations funding programs for their support of this work.

M. Skorobogatiy's e-mail address is maksim.skorobogatiy@polymtl.ca.

REFERENCES

1. V. M. Agranovich and D. L. Mills, *Surface Polaritons—Electromagnetic Waves at Surfaces and Interfaces* (North-Holland, 1982).
2. E. Kretschmann and Z. H. Raether, "Radiative decay of non-radiative surface plasmons excited by light," Z. Naturforsch., A: Phys. Sci. **23**, 2135–2136 (1968).
3. R. C. Jorgenson and S. S. Yee, "A fiber-optic chemical sensor based on surface plasmon resonance," Sens. Actuators B **12**, 213–220 (1993).
4. M. B. Vidal, R. Lopez, S. Aleggret, J. Alonso-Chamarro, I. Garces, and J. Mateo, "Determination of probable alcohol yield in musts by means of an SPR optical sensor," Sens. Actuators B **11**, 455–459 (1993).
5. R. Alonso, F. Villuendas, J. Tornos, and J. Pelayo, "New in-line optical fiber sensors based on surface plasmon excitation," Sens. Actuators A **37–38**, 187–192 (1993).
6. R. Alonso, J. Subias, J. Pelayo, F. Villuendas, and J. Tornos, "Single-mode, optical fiber sensors and tunable wavelength filters based on the resonant excitation of metal-clad modes," Appl. Opt. **33**, 5197–5201 (1994).
7. J. Homola, "Optical fiber sensor based on surface plasmon resonance excitation," Sens. Actuators B **29**, 401–405 (1995).
8. A. Trouillet, C. Ronot-Trioli, C. Veillas, and H. Gagnaire, "Chemical sensing by surface plasmon resonance in a multimode optical fibre," Pure Appl. Opt. **5**, 227–237 (1996).
9. A. J. C. Tubb, F. P. Payne, R. B. Millington, and C. R. Lowe, "Single-mode optical fibre surface plasma wave chemical sensor," Sens. Actuators B **41**, 1770–1771 (1997).
10. J. Homola, R. Slavik, and J. Ctyroky, "Interaction between fiber modes and surface plasmon wave: spectral properties," Opt. Lett. **22**, 1403–1405 (1997).
11. R. Slavik, J. Homola, and J. Ctyroky, "Single-mode optical fiber surface plasmon resonance sensor," Sens. Actuators B **54**, 74–79 (1999).
12. A. Diez, M. V. Andres, and J. L. Cruz, "In-line fiber-optic sensors based on the excitation of surface plasma modes in metal-coated tapered fibers," Sens. Actuators B **73**, 95–99 (2001).
13. M. Piliarik, J. Homola, Z. Manikova, and J. Ctyroky, "Surface plasmon resonance based on a polarization-maintaining optical fiber," Sens. Actuators B **90**, 236–242 (2003).
14. D. Monzon-Hernandez, J. Villatoro, D. Talavera, and D. Luna-Moreno, "Optical-fiber surface-plasmon resonance sensor with multiple resonance peaks," Appl. Opt. **43**, 1216–1220 (2004).
15. D. Monzon-Hernandez, and J. Villatoro, "High-resolution refractive index sensing by means of a multiple-peak surface plasmon resonance optical fiber sensor," Sens. Actuators B **115**, 227–231 (2006).
16. H. Suzuki, M. Sugimoto, Y. Matsuiand, and J. Kondoh, "Fundamental characteristics of a dual-colour fibre optic SPR sensor," Meas. Sci. Technol. **17**, 1547–1552 (2006).
17. J. Ctyroky, F. Abdelmalek, W. Ecke, and K. Usbeck, "Modelling of the surface plasmon resonance waveguide sensor with Bragg grating," Opt. Quantum Electron. **31**, 927–941 (1999).
18. A. Trouillet, C. Ronot-Trioli, C. Veillas, and H. Gagnaire, "Chemical sensing by surface plasmon resonance in a multimode optical fibre," Pure Appl. Opt. **5**, 227–237 (1995).
19. J. Ctyroky, J. Homola, P. V. Lambeck, S. Musa, H. J. W. M. Hoekstra, R. D. Harris, J. S. Wilkinson, B. Usievich, and N. M. Lyndin, "Theory and modelling of optical waveguide sensors utilising surface plasmon resonance," Sens. Actuators B **54**, 66–73 (1999).
20. M. Weisser, B. Menges, and S. Mittler-Neher, "Refractive index and thickness determination of monolayers by multi mode waveguide coupled surface plasmons," Sens. Actuators B **56**, 189–197 (1999).
21. B. D. Gupta and A. K. Sharma, "Sensitivity evaluation of a multi-layered surface plasmon resonance-based fiber optic sensor: a theoretical study," Sens. Actuators B **107**, 40–46 (2005).
22. M. Skorobogatiy and A. Kabashin, "Plasmon excitation by the Gaussian-like core mode of a photonic crystal waveguide," Opt. Express **14**, 8419–8424 (2006).
23. M. Skorobogatiy and A. Kabashin, "Photon crystal waveguide-based surface plasmon resonance biosensor," Appl. Phys. Lett. **89**, 143518 (2006).
24. B. T. Kuhmley, K. Pathmanadavel, and R. McPhedran,

"Multipole analysis of photonic crystal fibers with coated inclusions," Opt. Express **14**, 10851–10864 (2006).
25. A. Hassani and M. Skorobogatiy, "Design of the microstructured optical fiber-based surface plasmon resonance sensors with enhanced microfluidics," Opt. Express **14**, 11616–11621 (2006).
26. P. J. A. Sazio, "Microstructured optical fibers as high-pressure microfluidic reactors," Science **311**, 1583–1586 (2006).
27. J. A. Harrington, "A review of IR transmitting, hollow waveguides," Fiber Integr. Opt. **19**, 211–217 (2000).
28. N. Takeyasu, T. Tanaka, and S. Kawata, "Metal deposition deep into microstructure by electroless plating," Jpn. J. Appl. Phys., Part 1 **44**, 1134–1137 (2005).
29. C. M. B. Cordeiro, M. A. R. Franco, G. Chesini, E. C. S. Barretto, R. Lwin, C. H. B. Cruz, and M. C. J. Large, "Microstructured-core optical fibre for evanescent sensing applications," Opt. Express **14**, 13056–13066 (2006).
30. K. Kurihara, K. Nakamura, E. Hirayama, and K. Suzuki, "An absorption-based surface plasmon resonance sensor applied to sodium ion sensing based on an ion-selective optode method," Anal. Chem. **74**, 6323–6329 (2002).
31. S. J. Al-Bader and M. Imtaar, "Optical fiber hybrid-surface plasmon polaritons," J. Opt. Soc. Am. B **10**, 83–88 (1993).
32. S. Patkovsky, A. Kabashin, and M. Meunier, "Near-infrared surface plasmon resonance sensing on a Si platform with nanoparticle-based signal enhancement," Opt. Mater. **27**, 1093–1096 (2005).
33. L. O. Cinteza, T. Y. Ohulchanskyy, Y. Sahoo, E. J. Bergey, R. K. Pandey, and P. N. Prasad, "Diacyllipid micelle-based nanocarrier for magnetically guided delivery of drugs in photodynamic therapy," Mol. Pharmacol. **3**, 415–423 (2006).
34. J. Homola, S. S. Yee, and G. Gauglitz, "Surface plasmon resonance sensors: review," Sens. Actuators B **54**, 3–15 (1999).